RSC Advances

PAPER

View Article Online
View Journal | View Issue

Cite this: *RSC Adv.*, 2025, **15**, 2645

A cost-effective and innovative detector for iron ions†

Yanhui Guo, Jiayi Zhu, Yumei Dai, Long Chen, Weibing Li, Zihang Yuan, Jie Zhou and En Tang *

Severe environmental contamination can result from high concentrations of iron ions, which can have a detrimental impact on human health and well-being. Consequently, it is imperative to develop novel materials that can address environmental issues. Metal–organic frameworks (MOFs) possess unique properties that render them efficient fluorescent probes for the rapid and precise detection of these pollutants. A diverse array of MOF probes have been developed to detect iron ions. Nevertheless, their practical application is significantly impeded by the high production cost, which is a critical factor. This raises the question: why not implement a cost-effective, sensitive detector instead? Our research group has developed a novel MOF material, $[Zn_2(bpy)(APA)_2(H_2O)]_n$, that is specifically designed for MOF-based "off" sensors in aqueous media. This material not only demonstrates high sensitivity, and is manufactured from low-cost raw materials, but it also holds significant commercial potential, with production costs that are 98.4% lower than those of existing alternatives.

Received 13th November 2024
Accepted 20th January 2025

DOI: 10.1039/d4ra08065c

rsc.li/rsc-advances

Introduction

The processes of urbanization and industrialization are substantial indicators of a nation's strength. Nevertheless, these have a negative effect on the environment, resulting in increased pollution.[1–3] Additionally, the existence of humans and other living organisms is directly impacted by the global environment. Water pollution is considered one of the most significant issues in recent times, among the various forms of environmental pollution. Although there are numerous sources of water pollution, chemical sources are considered to be among the most toxic and detrimental. A variety of contaminants, such as heavy metals, anions, dyes, pesticides, and even high concentrations of radioactive substances, are present in the substantial quantities of sewage that are discharged. Among these, pollutants containing metal ions are of growing concern due to their persistent nature and inability to biodegrade. Consequently, it is crucial to monitor and detect metal cations to address these environmental challenges effectively.

Fe^{3+} ions are essential for biological systems; however, an excessive ingestion can lead to the development of metabolic disorders and adverse health effects.[4] At present, there are a multitude of methods for detecting metal cations. Nevertheless, the instruments are intricate, and the techniques are costly.[5–7] As a result, the emergence of swift and highly selective detection technology is imminent. MOFs are not only compliant with these conditions, they also possess the potential to be beneficial in several applications.[8–15] Trace metal ions were directly detected using spectrophotometry, which utilizes the unique 'on' and 'off' mechanisms characteristic of MOFs. Nevertheless, the practical application of MOFs is significantly impeded by their high manufacturing cost. Consequently, a new low-cost MOF material has emerged as the optimal choice for current advancements. Numerous MOFs have been developed for the purpose of detecting Fe^{3+}, and a significant number have been demonstrated to be effective as Fe^{3+} detectors.[16–18] In contrast, the experimental team successfully synthesized a new material using simple methods and a minimal number of inexpensive chemicals. The solvothermal method was employed to synthesize a new luminescent MOF with zinc ions as the central unit, with raw materials including 4,4′-bipyridine (bipy), 5-acetylaminoisophthalic acid (H_2APA), and $ZnSO_4 \cdot 7H_2O$.

Experimental

Materials

Zinc sulfate heptahydrate (99%) was supplied by Sinopharm Chemical Reagent Co, along with 5-amino-1,3-benzenedicarboxylic acid (99%) and acetic anhydride (99%). Additional reagents were obtained from Aladdin Reagents Ltd, including 4,4′-bipyridine (99%), *N*,*N*-dimethylformamide (DMF, 99.5%), methanol (99.5%), acetonitrile (99.5%), and concentrated sulfuric acid (98%). All reagents were used without further purification except for 5-amino-1,3-benzenedicarboxylic acid, which was modified.

Minnan Science and Technology University, China. E-mail: tangen@mku.edu.cn

† Electronic supplementary information (ESI) available. CCDC 2396827. For ESI and crystallographic data in CIF or other electronic format see DOI: https://doi.org/10.1039/d4ra08065c

Synthesis of Zn-MOFs

A mixture containing 0.0949 g of $ZnSO_4 \cdot 7H_2O$ (0.33 mmol), 0.0468 g of 4,4′-bipy (0.3 mmol), and 0.067 g of H_2APA (0.3 mmol, schematic diagram of the synthesis of H_2APA see Fig. S1†) in 6 mL of deionized water and 1 mL of DMF was placed in a Teflon-lined stainless steel autoclave and heated at 120 °C for 12 hours. Afterward, the mixture was cooled to room temperature and filtered, yielding colorless, flaky Zn-MOF crystals.

Detection of Fe^{3+} with Zn-MOFs

An aqueous dispersion of Zn-MOFs at a concentration of 747.2 mg L^{-1} was added to ferric chloride solutions of varying concentrations. After thorough mixing and allowing the solutions to stabilize for five minutes, their fluorescence properties were measured. To further demonstrate the Zn-MOFs' excellent immunity and high selectivity toward Fe^{3+}, a series of selectivity experiments were conducted under the same conditions using a range of chloride salts, including $CaCl_2$, NaCl, KCl, $CdCl_2$, $CoCl_2$, $MnCl_2$, $CuCl_2$, and $LaCl_3$.

Characterization

Photoluminescence spectra and CIE coordinates of Zn-MOFs were obtained using an FL-4700 steady-state fluorescence spectrophotometer and CIE 1931 software. The X-ray crystal structure was determined by collecting crystals on a Bruker APEX CCDC diffractometer equipped with a graphite monochromator and Mo-Kα radiation ($\lambda = 0.71073$ Å). X-ray powder diffraction (XRD XB5100) was employed to analyze the phase composition of the samples. Fourier transform infrared (FTIR) spectra were recorded using an IRAffinity-IS infrared spectrometer (Nicole, USA). The microscopic morphology was examined with a TM-3000 scanning electron microscope (SEM, $V = 15$ kV, Japan), while the pore size of the samples was measured using BET analysis. Additionally, the dimensions of Zn-MOFs were assessed through dynamic light scattering (DLS).

Results and discussion

Structural description of Zn-MOFs

Single-crystal X-ray analysis revealed that the material possesses a monoclinic crystal system with a space group of $P2_1/c$. The structure is comprised of Zn^{2+} ions, several protonated APA, 4,4′-bipyridine ligands, and ligand water molecules, resulting in a novel structural configuration (Fig. 1a). In this arrangement, three distinct oxygen atoms from APA^{2-} coordinate with Zn1 and the nitrogen atom of 4,4′-bipyridine. The APA^{2-} not only chelates with Zn1 but also exhibits monodentate coordination. Simultaneously, Zn2 is coordinated by oxygen atoms from three different APA^{2-} ligands, nitrogen atoms within the framework, and oxygen atoms from ligand water molecules. This leads to the formation of a two-dimensional metal network among the Zn^{2+} ions through the carboxylate oxygen atoms on the APA^{2-} (Fig. 1b). As depicted in Fig. 1c, the nitrogen atom in the 4,4′-bipyridine ligand forms a coordination bond with the zinc atom, creating a network framework characterized by numerous voids.

Characterisation of Zn-MOF

To verify the properties of Zn-MOFs, we conducted powder X-ray diffraction (PXRD) experiments. As shown in Fig. S2,† the positions of the principal peaks in the theoretical and experimental PXRD spectra align closely, indicating that the Zn-MOFs exhibit high crystal purity. The PXRD of Zn-MOF after immersion in different solvents for 24 hours is shown as Fig. S3.† The positions of the main peaks before and after immersion in various solvents match closely, indicating the high stability of the Zn-MOF structure. The FTIR spectra (Fig. S4†) reveal the absence of a strong absorption peak near 1700 cm^{-1}, suggesting that the carboxyl group in the H_2APA ligand has been completely deprotonated. The peak at 1612 cm^{-1} corresponds to the antisymmetric stretching vibrational absorption of the carboxyl group. Additionally, the symmetric stretching vibrational absorption peaks at 1548 cm^{-1} and 1379 cm^{-1} represent the symmetric stretching of the carboxyl group. The difference between the symmetric and antisymmetric stretching vibrations of the carboxyl group is 233 cm^{-1} and 64 cm^{-1}, respectively. Upon observing that the values of $\Delta[\nu_{as} - \nu_s]$ is lower than 200 cm^{-1}, the carboxylate moiety is postulated to be coordinated in a bidentate mode. In contrast, when the value of $\Delta[\nu_{as} - \nu_s]$ exceeds 200 cm^{-1}, the carboxylate moiety is considered to be coordinated in a monodentate fashion. The $\Delta[\nu_{as} - \nu_s]$ of 233 cm^{-1} and 64 cm^{-1} indicate the presence of monodentate and bidentate coordination in the structure, which is consistent with the crystal structure. As depicted in Fig. 2, the Zn-MOFs exhibit a gem-like appearance, correlating with their three-dimensional structure. As is evident from the figure, Zn-MOF represents a novel micron-sized material. The pore size characteristics of the Zn-MOFs and the particle diameter distribution in solution were analyzed using BET and DLS techniques, as illustrated in Fig. S5.† Thermogravimetric analysis was employed to assess the thermal stability of the Zn-MOFs (Fig. S6†). No weight loss was observed up to 200 °C. The first weight loss, amounting to 3.967%, occurred between 200 °C and 370 °C, attributed to the loss of H_2O molecules. The theoretical weight loss for the end-group coordination is 2.41%, with the framework remaining stable until 370 °C. Beyond this temperature, the anhydrous structure begins to decompose, resulting in a final residue that can be attributed to the formation of ZnO. The specific surface area of Zn-MOFs was calculated to be 2.36874 $m^2\ g^{-1}$, with the pore adsorption curve indicating a pore width of 3.59 nm and the desorption curve indicating a pore width of 3.53 nm. The dimensions of Zn-MOFs were quantified using DLS, revealing that their size distribution in aqueous solution was approximately 297 nm.

The fluorescence properties of Zn-MOFs

The unique configuration of the H_2APA ligand provides an intriguing basis for exploring its effects on fluorescence. The liquid fluorescence spectra of the H_2APA ligand, 4,4′-bipyridine, and their corresponding Zn-MOFs were recorded at room

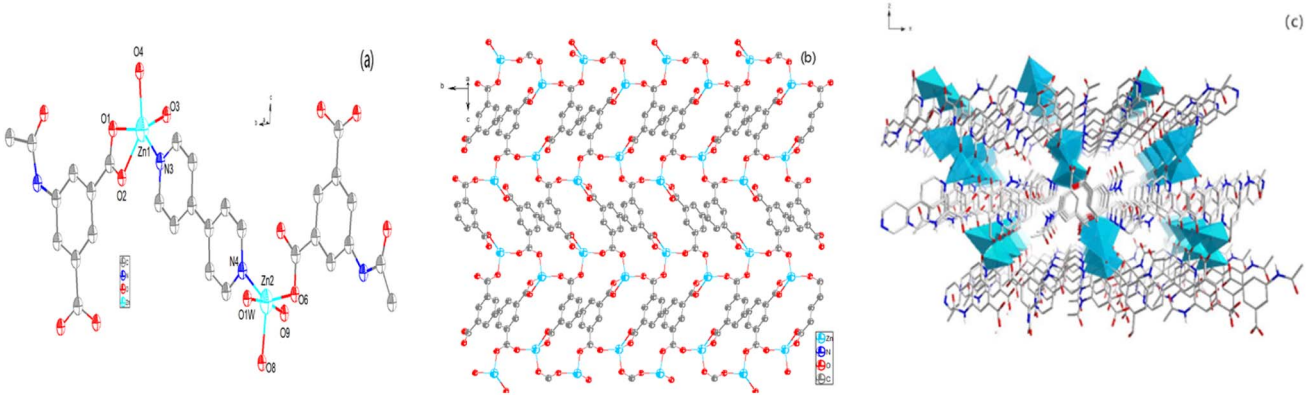

Fig. 1 (a) The coordination environment around Zn(II) ions in MOF 1. Symmetry codes: #1: 1 – *x*, 2.5 – *y*, 0.5 + *z*; #2: 1 – *x*, 2 – *y*, –*z*; #3: *x*, 0.5 – *y*, – 0.5 + *z*; (b) stacking diagram of Zn-MOFs, showing a view of the 2-D network formed by APA-Zn(II); (c) the figure illustrates the pore structure of the three-dimensional supramolecular framework, with the zinc-centered subunit depicted in blue.

temperature and are presented in Fig. 3a. All three samples were excited at 280 nm. The H_2APA ligand displayed fluorescence at 351 nm, likely due to a $\pi^* \rightarrow n$ or $\pi^* \rightarrow \pi$ transition. In contrast, when excited at 280 nm, the Zn-MOFs exhibited an emission peak at 465 nm. This emission can be attributed to ligand–metal charge transfer,[19,20] which plays a significant role in Zn-MOFs. Notably, the H_2APA ligand and its derivatives exhibited a distinct color change from blue to cyan (Fig. 3b), while the CIE coordinates shifted from (0.1506, 0.0688) to (0.1334, 0.1453).

Fluorescence sensing experiments

Initially, 2.7 mL of a 0.001 mol L^{-1} complex sample was mixed with 0.3 mL of a 0.001 mol L^{-1} $M(Cl)_n$ solution (where M = Ca^{2+}, K^+, Mn^{2+}, Fe^{3+}, Co^{2+}, Na^+, Cu^{2+}, Cd^{2+}, La^{3+}). This mixture was sonicated for 60 minutes to create a well-distributed suspension, and the fluorescence spectra of the suspensions were subsequently measured. The actual fluorescence plot for all chlorinated salts is shown as Fig. S7,† which demonstrates high sensitivity for Fe^{3+}. Fig. 4a displays the fluorescence intensity (λ_{ex} = 280 nm) of Zn-MOFs in DMF solutions containing various cations. Due to their excellent fluorescence response and high selectivity for Fe^{3+}, the Zn-MOFs synthesized in this study are expected to serve as highly sensitive fluorescent probes for Fe^{3+} detection. To assess the sensitivity of Zn-MOFs to Fe^{3+} ions, Fe^{3+} solutions of varying concentrations were introduced into the suspension, followed by fluorescence intensity measurements of the Zn-MOFs. As illustrated in Fig. 4b, the emission intensity of the Zn-MOF suspensions gradually decreased as the concentration of Fe^{3+} increased from 0 to 1100 μM at 0.01 mol L^{-1}. The quenching efficiency of Fe^{3+} ions was quantified using the Stern–Volmer equation $(I_0/I) = K_{SV}[A] + 1$, where I_0 is the fluorescence intensity of the sample, I

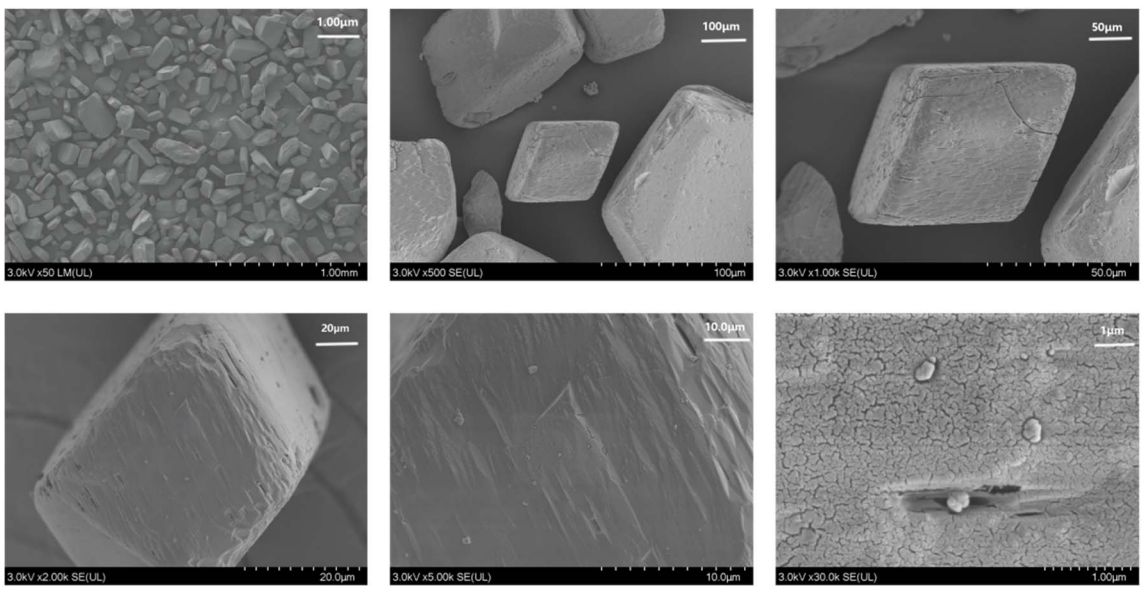

Fig. 2 Scanning electron micrographs of zinc metal–organic frameworks (Zn-MOFs).

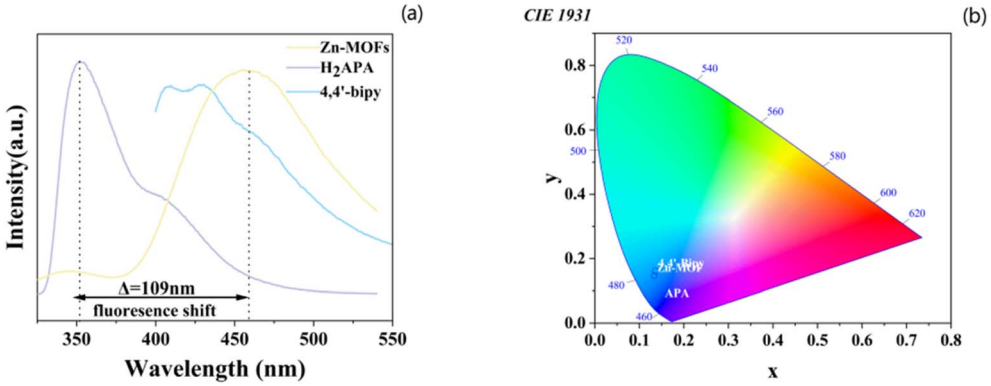

Fig. 3 (a) Fluorescence spectra of H_2APA, 4,4′-bipyridine ligand, and Zn-MOF (λ_{ex} for all samples at 280 nm); (b) CIE-1931 color diagrams for H_2APA, 4,4′-bipyridine, and related Zn-MOFs.

is the fluorescence intensity after the addition of metal ions, [A] is the molar concentration of Fe^{3+}, and K_{SV} is the quenching constant.[21–23] Notably, the K_{sv} value for the Zn-MOFs in response to Fe^{3+} at low metal ion concentrations was 0.994×10^4 M^{-1} ($R^2 = 0.9999$).

$$I_0/I = K_{sv}[A] + 1$$

Using the calculated K_{sv} value, the limit of detection (LOD)[24,25] and limit of quantification (LOQ) for the fluorescent probe can be determined using the following formulas:[26,27]

$$LOD = 3\sigma/K_{sv}$$

$$LOQ = 10\sigma/K_{sv}$$

The results indicated that the LOD and LOQ of Zn-MOFs for Fe^{3+} were 5.619×10^{-6} and 1.895×10^{-5}, respectively, both of which are lower than the primary standard of 0.3 mg L^{-1} for Fe^{3+} in the China Comprehensive Wastewater Emission Standard (GB3838-2002). Thus, Zn-MOFs serve as a novel fluorescent probe capable of accurately detecting Fe^{3+} in wastewater.

In addition to demonstrating fluorescence sensing capabilities, it is crucial to evaluate the anti-interference ability of the material in practical applications. Therefore, eight chloride salts were selected to assess their impact on the fluorescence intensity of Zn-MOFs at a constant concentration of 0.1 mol L^{-1}. As shown in Fig. 4c, the fluorescence intensity of Zn-MOFs was notably influenced. It is important to note that introducing these metal salts into the Zn-MOFs mixture in the presence of ferric chloride resulted in a rapid decline in fluorescence intensity. However, this effect was less pronounced than when ferric chloride was added alone, suggesting that Zn-MOFs exhibit a high selectivity and interference resistance level in detecting Fe^{3+} as fluorescent probes, especially compared to other chloride salts, with limits of detection (LOD) values similar to those of other MOFs. Furthermore, our material offers distinct advantages, positioning it competitively in the market at the same preparatory cost.[28,29]

Mechanism of fluorescence quenching

To conduct an in-depth analysis of the quenching phenomenon, we juxtaposed the excitation spectrum of Zn-MOF with the UV-Vis absorption spectra of chlorinated salts (Fig. 5). In Fig. 5, only the UV–Vis spectrum of ferric chloride shows an absorption band that coincides with the excitation range of Zn-MOF. These discoveries distinctly signify the energy transduction between the MOF framework and ferric chloride, which

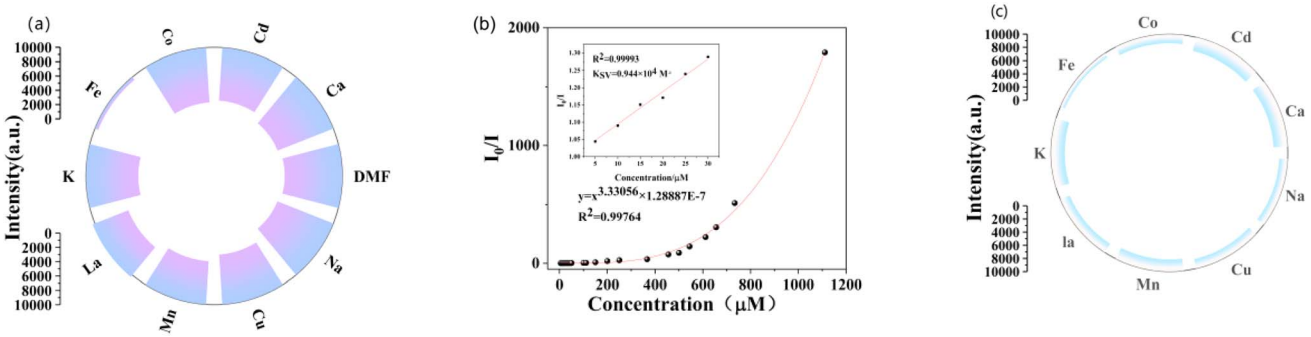

Fig. 4 (a) Fluorescence intensity after the addition of metal quenchers; (b) the Stern–Volmer diagram of Zn-MOFs at increasing concentrations of Fe^{3+} ions, with the inset displaying S–V plots of Zn-MOFs at 5–30 μmol of Fe^{3+} ions; (c) fluorescence intensity of various metal salts following the addition of Fe^{3+}.

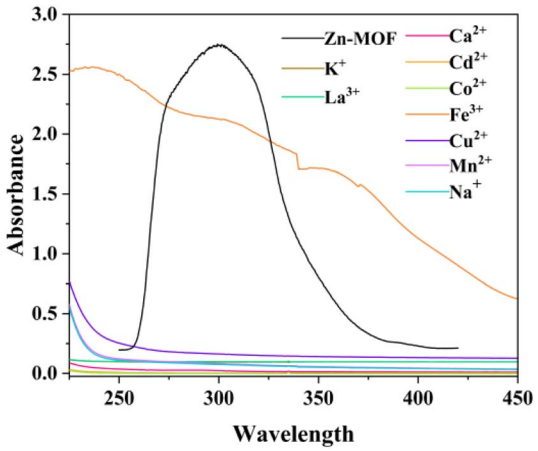

Fig. 5 Ultraviolet spectrum of a chloride salt and excitation spectrum of Zn-MOFs.

ultimately culminates in the selective photoluminescence quenching of Zn-MOF. Such a remarkable overlap between the UV-Vis absorption spectra of the targeted ferric chloride and the excitation profile of Zn-MOF also accentuates the probable contribution of the inner filter effect to PL quenching.[30–32]

Conclusions

In conclusion, we successfully synthesized a Zn(II)-based luminescent coordination polymer using 4,4′-bipyridine (bpy) and H_2APA under hydrothermal conditions. The synthesis resulted in a novel three-dimensional structure formed by the linkage of the bipyridine ligand. Additionally, Zn-MOFs are identified as a cost-effective material with significant potential for water detection, which also has high sensitivity and effective fluorescent sensing capabilities, and the potential sensing mechanism was thoroughly elucidated through ultraviolet-visible spectroscopy. Zn-MOFs can serve as fluorescent probes for accurate iron measurements, underscoring their commercial value, while also offering new insights into the practical applications of fluorescent probes.

Data availability

All data supporting the findings of this study are available within the paper and its ESI.† The data used in this study were collected during the Fujian Province First-Class Undergraduate Program Construction Point (Applied Chemistry) (SJZY-2020-01) research project conducted by Minnan Science and Technology University. Crystallographic data for CCDC-2396827 has been deposited at the 2396827 under CCDC and can be obtained from **https://www.ccdc.cam.ac.uk**.†

Author contributions

The authors have no conflicts of interest to declare with respect to the research, authorship and publication of this article.

Conflicts of interest

There are no conflicts to declare.

Acknowledgements

This work was supported by (1) Fujian Province First-Class Undergraduate Program Construction Point (Applied Chemistry) (SJZY-2020-01), (2) Innovation and Entrepreneurship in Fujian Province (S202412992017).

Notes and references

1 Z. Y. Li, P. Y. Zhu, H. Chang, Z. Z. Hou, M. L. Shao and B. Zhai, *Dyes Pigm.*, 2022, **207**, 110719, DOI: **10.1016/j.dyepig.2022.110719**.
2 P. Izadi, P. Izadi, R. Salem, S. A. Papry, S. Magdouli, R. Pulicharla and S. K. Brar, *Environ. Pollut.*, 2020, **267**, 115370, DOI: **10.1016/j.envpol.2020.115370**.
3 T. Islamoglu, Z. Chen, M. C. Wasson, C. T. Buru, K. O. Kirlikovali, U. Afrin, M. R. Mian and O. K. Farha, *Chem. Rev.*, 2020, **120**, 8130–8160, DOI: **10.1021/acs.chemrev.0c00224**.
4 Z. Zhou, M. C. Shang, Z. H. Yao and J. J. Zhang, *Dyes Pigm.*, 2022, **198**, 110016, DOI: **10.1016/j.dyepig.2022.110016**.
5 N. Zhang, D. Zhang, J. Zhao and Z. Xia, *Dalton Trans.*, 2019, **48**, 6794–6799, DOI: **10.1039/C9DT01363A**.
6 D. D. Yang, L. P. Lu, S. S. Feng and M. L. Zhu, *Dalton Trans.*, 2020, **49**, 7514–7524, DOI: **10.1039/D0DT01684H**.
7 J. Zhao, Y. N. Wang, W. W. Dong, Y. P. Wu, D. S. Li and Q. C. Zhang, *Inorg. Chem.*, 2016, **55**, 3265–3271, DOI: **10.1021/acs.inorgchem.5b02717**.
8 X. J. Ma, Y. T. Chai, P. Li and B. Wang, *Acc. Chem. Res.*, 2019, **52**, 1461–1470, DOI: **10.1021/acs.accounts.9b00277**.
9 Y. L. Yang, Y. R. Wang, L. Z. Dong, Q. Li, L. Zhang, J. Zhou, S. N. Sun, H. M. Ding, Y. Chen, S. L. Li and Y. Q. Lan, *Adv. Mater.*, 2022, **34**, 2206706, DOI: **10.1002/adma.202206706**.
10 L. K. Thompson and L. N. Dawe, *Coord. Chem. Rev.*, 2015, **289–290**, 13–31, DOI: **10.1016/j.ccr.2015.06.003**.
11 A. Bavykina, N. Kolobov, I. S. Khan, J. A. Bau, A. Ramirez and J. Gascon, *Chem. Rev.*, 2020, **120**, 8468–8535, DOI: **10.1021/acs.chemrev.0c00274**.
12 N. S. Bobbitt, M. L. Mendonca, A. J. Howarth, T. Islamoglu, J. T. Hupp, O. K. Farha and R. Q. Snurr, *Chem. Soc. Rev.*, 2017, **46**, 3357–3385, DOI: **10.1039/C6CS00737A**.
13 M. A. Somnath and K. A. Siddiqui, *Dalton Trans.*, 2023, **52**, 3643–3660, DOI: **10.1039/D3DT00555J**.
14 Y. N. Zhou, *et al.*, *Inorg. Chem.*, 2021, **60**, 17303–17314, DOI: **10.1021/acs.inorgchem.1c02572**.
15 C. Lin, *et al.*, *Inorg. Chem.*, 2021, **60**, 16803–16809, DOI: **10.1021/acs.inorgchem.1c02773**.
16 Y. Y. Zhao, *et al.*, *Microporous Mesoporous Mater.*, 2023, **362**, 112764, DOI: **10.1016/j.micromeso.2023.112764**.
17 L. Ma, Y. Y. Liu and F. Su, *J. Solid State Chem.*, 2023, **269**, 65–71, DOI: **10.1016/j.jssc.2019.02.010**.
18 F. Su, J. Liu, Z. Zhang, *et al.*, *Acta Crystallogr., Sect. C:Struct. Chem.*, 2019, **75**, 141–149, DOI: **10.1107/S2053229619000390**.

19 Y. N. Zhou, *et al.*, *Inorg. Chem.*, 2021, **60**, 17303–17314, DOI: 10.1021/acs.inorgchem.1c02572.
20 C. Lin, *et al.*, *Inorg. Chem.*, 2021, **60**, 16803–16809, DOI: 10.1021/acs.inorgchem.1c02773.
21 A. Y. Yu and X. C. Wang, *J. Mol. Struct.*, 2024, **1295**, 136624, DOI: 10.1016/j.molstruc.2023.136624.
22 Y. X. Ma, M. C. Zhu, Y. Zhang, Y. G. Sun and S. Y. Wu, *J. Solid State Chem.*, 2022, **316**, 123598, DOI: 10.1016/j.jssc.2022.123598.
23 M. J. Lee, A. P. Tiwari, T. H. Ko and H. Y. Kim, *J. Lumin.*, 2022, **249**, 119029, DOI: 10.1016/j.jlumin.2022.119029.
24 S. W. Thomas, G. D. Joly and T. M. Swager, *Chem. Rev.*, 2007, **107**, 1339–1386, DOI: 10.1021/cr068123a.
25 C. H. Zhang, *et al.*, *J. Mater. Chem. C*, 2017, **5**, 8999–9004, DOI: 10.1039/C7TC03013A.
26 K. Abha, *et al.*, *Sens. Actuators, B*, 2019, **282**, 300–308, DOI: 10.1016/j.snb.2018.11.064.
27 C. H. Zhan, *et al.*, *CrystEngComm*, 2021, **23**, 2788–2792, DOI: 10.1039/D1CE00316B.
28 S. K. Panda, S. Mishra and A. K. Singh, *Dalton Trans.*, 2021, **50**, 7139, DOI: 10.1039/D1DT00835A.
29 X. X. Jing, J. Liu, M. Guo, G. Chen, G. Ren, J. Li, H. Qin, Z. Yao, Y. Wan, W. Song, H. Zeng, F. Yang, D. Zhao and K. Hu, *J. Lumin.*, 2023, **200**, 123–130, DOI: 10.1016/j.jlumin.2023.06.001.
30 R. Minmini, S. Naha and S. Velmathi, *Sens. Actuators, B*, 2017, **251**, 644–649, DOI: 10.1016/j.snb.2017.05.030.
31 F. G. M. Mauricio, J. Y. R. Silvab, M. Talhavinid, S. A. Júnior and I. T. Weber, *Microchem. J.*, 2019, **150**, 104037, DOI: 10.1016/j.microc.2019.104037.
32 S. Dutta, W. Mandal, A. V. Desai, G. K. Dam, S. Mukherjee, S. Fajal and S. K. Ghosh, *Mol. Syst. Des. Eng.*, 2023, **8**, 1483, DOI: 10.1039/d3me00008g.